A Method for Jet Noise Using Large-Eddy Simulation

Aiqin Li and Jiecheng Yu

Beijing Institute of Petro-chemical Technology, Beijing 102617,China

Abstract

In order to verify the feasibility of the method of numerical simulation of supersonic noise, the flow field and noise at far field of a small solid fuel rocket engine F tested by National Aeronautics and Space Administration's Langley Research Center (NASA) was simulated by computational fluid dynamics (CFD) and computational aeroacoustics (CAA). The conjunction with large eddy simulation and FW-H integral method is adopted to simulate spectrums of the noise. The conjunction with large eddy simulation and Möhring sound analogy is adopted to predict the direction of the noise at the near-field. Comparing the result with the experimental data, the flow field coincides well, and in the sound field, the low and medium-frequency sound pressure level coincides well too, and the high-frequency sound pressure level is slightly lower than the estimated value. The error of overall sound pressure level of the measure point is small. The sound field resulted by high temperature, high pressure and high velocity fluid is simulated successfully.

Keywords: rocket engine; jet noise; numerical simulation

1. Introduction

When a rocket is launching, the intense turbulent flow formed by the drastic blend of the supersonic high temperature gas flow with the relatively static air will result in supersonic jet noise, the sensing elements installed near rocket engine will be disturbed even disabled, which maybe cause serious negative effects. The noise also damage shooter's hearing organ, visual organ and the physiology. Therefore, it is necessary to predict accurately noise field during the process of rocket design in order to protect device and staff as much as possible.

The experimental method and theoretical analysis are used to predict the noise of the rocket launching. The experimental method is restricted due to the high cost and bad performance of the transducer at high temperature. Otherwise, the theoretical analysis become the main method to predict the noise due to its high repeatability and low cost, *etc*. So exploring and verifying the effectiveness of theoretical analysis to simulate the high temperature and high speed jet noise is very important when developing new low-noise safe engine. When rocket launching, the rocket engine will jet high temperature, high pressure, high speed gas flow, its pressure at exit is 10 billion times bigger than the pressure of recognized noise. Thus the high accuracy is required when the numerical simulation performed, which will result in bad convergence, long computation period, bad stability.

Usually, supersonic noise is investigated by the combination of the flow field simulation (Computational Fluid Dynamics, CFD) and sound field calculation (Computational Aeroacoustics CAA) Firstly, we can obtain the time domain data by the flow field simulation, then the time domain data is transformed to the frequency domain data by fast Fourier transformation. Lastly, the near-field and far-field distribution of the noise are simulated by sound field calculation.

At present, there are three numerical simulation methods to predict supersonic flow field, they are Direct Numerical Simulation (DNS) method, Linearized Euler Equations

(LEE) and Large Eddy Simulation (LES). The DNS method is used to predict the supersonic flow field by solving the full, unsteady, compressible N-S equations directly, which can only be applied in the case of low Reynolds number turbulence flow due to the limit of the computer resource. The LEE method is not enough accurate because it neglects effect of viscosity and nonlinearity, which can be applied to explain some flow mechanisms. The LES is next best simulating method, by which the instantaneous turbulent flow is decomposed into large eddy and small eddy through filtering method, and large eddy is solved directly the N-S equations while small eddy is simulated by sub-grid scale model. The LES method has been applied widely to predict jet noise since 2001, most cases focus on low Mach number, low Reynolds number or free-jet fluid with low to middle temperature due to lacking of experimental data or the limit of computer resource, while the full 3-D LES simulation for the high temperature, high pressure, high speed gas flow is seldom.

Sound field simulation originated from acoustic analogy created by Lighthill in 1952. Kirchhoff integral method and Ffowcs Williams Hawkings (FW-H) surface integration based on it were developed later[1, 2]. Density is regarded as major variable of sound in the above three methods. In 2010, Möhring[3] deduced Möhring acoustic analogy from the N-S equations in which enthalpy is regarded as major variable.

In this paper, the far-field noise will be simulated by using the LES and FW-H method, and the directivity of noise was simulated by using the LES and Möhring acoustic analogy, also the convergent approach to simulate outer flow field by using the LES method will be determined. It is the first try to simulate the directivity of noise field of rocket engine by combination the LES method with the Möhring acoustic analogy, and the numerical simulation of sound field formed by high temperature, high pressure and high-speed fluid is achieved successfully.

2. Verification Model

Jean Varnier[4] had been measured the flow field and sound field of a small solid fuel Rocket engine F when it remain static, a convergent-divergent nozzle was used in the rocket engine F (see Figure 1), its structure and working parameter show in Table 1.
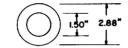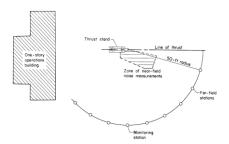

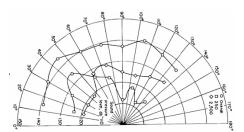**Figure 1. The Nozzle's Schematic Diagram Of The Rocket Engine F [5]**

W.H.Mayes *et al*.[5] fixed rocket engine F on experiment table to do static firing. The engine was installed horizontally on the experiment Table 3.5 feet above the ground with central axis parallel to the ground. See Figure 2 for test methods for near-field and far-field noise. Near-field noise sensors were linear layout while far-field sensors were semicircular layout, its radius is 50 feet, and the center locates at the exit center of the nozzle, and each noise sensor was placed from 15 deg to 135 deg in every 15 deg.
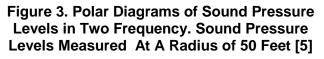
Table 1. Structure and Working Parameters of the Rocket Engine F [4]

Throat area, "	Exit area, "	Thrust, N	Chamber pressure, kPa	Exit pressure, kPa	Exit speed, m/s	Exit Mach number
1.50	2.88	7342	5470	250	2011	2.6

Figure 2. Plan View Sketch of Test Area, Showing Measurement Stations for Rocket-Engine Noise Surveys [5]

Figure 3. Polar Diagrams of Sound Pressure Levels in Two Frequency. Sound Pressure Levels Measured At A Radius of 50 Feet [5]

Shown in Figure 3 are polar diagram of sound pressure level and overall sound pressure level of measure points in two frequencies bands for rocket engine F. The far-field noise of which was obviously directional, while the overall sound pressure level was not obvious.

Shown in Table 2 are the value of sound pressure level of several noise frequencies collected by the sensors in 15deg and 30 deg.

Table 2. Engine F Sound Pressure Level Testing Value[5]

Azimuth Angle (deg)	Sound pressure level, db, for-						
	200 Hz	800 Hz	1000 Hz	2000 Hz	4000 Hz	8000 Hz	10000 Hz
15°	118	119	117	120	118	118	116
30°	130	123	118	125	122	120	118

3. Engine Noise Simulation

3.1. Flow Field Simulation

The governing equations of compressible turbulent flow for large eddy simulation can be deduced from the compressible N-S equations. A very complex solvable scale turbulent flow equation can be obtained by direct filtering of compressible N-S equations. Density weighted filtering (Favre filtering) [6] was used to obtain the following closure large eddy simulation equations of compressible turbulent flow.

$$G(x,x') = \begin{cases} 1/V & x' \in v \\ 0 & x' \text{ otherwise} \end{cases} \tag{1}$$

Favre filtered N-S equation is

$$\bar{\phi} = \frac{\overline{\rho\phi}}{\bar{\rho}} \tag{2}$$

filtered equation of continuity is

$$\frac{\partial \rho}{\partial t} + \frac{\partial}{\partial x_i}(p\bar{u}_j) = 0 \tag{3}$$

filtered momentum equation is

$$\frac{\partial}{\partial t}(\rho\bar{u}_i) + \frac{\partial}{\partial x_j}\left(\rho\bar{u}_i\bar{u}_j\right) = \frac{\partial}{\partial x_j}\left(\sigma_{ij}\right) - \frac{\partial\bar{p}}{\partial x_i} - \frac{\partial\tau_{ij}}{\partial x_j} \tag{4}$$

$$\sigma_{ij} \equiv [\mu(\frac{\partial u_i}{\partial x_j} + \frac{\partial u_j}{\partial x_i})] - \frac{2}{3}\mu\frac{\partial\bar{u}_i}{\partial x_i}\delta_{ij} \tag{5}$$

$$\tau_{ij} \equiv \rho \overline{u_i u_j} - \rho \overline{u}_i \overline{u}_j \tag{6}$$

filtered energy equation is

$$\frac{\partial \rho \overline{h}_s}{\partial t} + \frac{\partial \rho \overline{u}_i \overline{h}_s}{\partial r_i} - \frac{\partial \overline{p}}{\partial t} - \overline{u}_j \frac{\partial \overline{p}}{\partial x_i} - \frac{\partial}{\partial x_i}(\lambda \frac{\partial \overline{T}}{\partial x_i}) = -\frac{\partial}{\partial x_j} \rho \left(\overline{u_i h_s} - \overline{u}_i \overline{h}_s \right) \tag{7}$$

where, $\frac{\partial}{\partial x_j} \rho \left(\overline{u_i h_s} - \overline{u}_i \overline{h}_s \right)$ is sub-grid enthalpy flux; h_s is sensitive enthalpy; λ is

thermal con-ductivity. Sub-grid enthalpy flux is determined by equation (8):

$$\frac{\partial}{\partial x_j} \rho \left(\overline{u_i h_s} - \overline{u}_i \overline{h}_s \right) = -\frac{\mu_{SGS} C_p}{\mathrm{Pr}_{SGS}} \frac{\partial \overline{T}}{\partial x_j} \tag{8}$$

where, μ_{SGS} is sub-grid viscosity; Pr_{SGS} is sub-grid Prandtl number 0.85.

$$q_j = \frac{u_t \partial \phi}{\sigma_t \partial x_j} \tag{9}$$

where, μ_t is sub-grid viscosity of turbulent flow, determined by Smagorinsky-Lilly m o d e l . This LES sub-grid model can be obtained from the statistical results basically consistent with DNS.

$$\mu_t = \rho L_s 2 |\overline{S}| \tag{10}$$

$$L_s = \min(kd, C_s \Delta) \tag{11}$$

$$\Delta = V^{\frac{1}{3}} \tag{12}$$

where, L_s is sub-grid scale mixing length, which can be determined by equation (11); k is the von karman constant; d is the distance to the nearest wall; c_s is the Smagorinsky constant; Δ is the local grid scale, and the calculation was based on grid volume.

3.2. Sound Field Simulation

3.2.1. Ffowcs Williams-Hawkings (FW-H) Surface integration:

The sound source face during the process of the Ffowcs Williams-Hawkings (FW-H) surface integration calculation can be set at any position in flow field including the non-linear area of the jet flow, which can save computer resources. FW-H surface integration do not limit linearized and non-viscous undulatory spread, and can reduce numerical dispersion and dissipation during the process of the wave transmission to the surface. FW-H equation was a non-homogeneous wave equation, which is deduced from the continuity equation and N-S equation.

$$\frac{1}{a_0^2} \frac{\partial^2 p'}{\partial t^2} - \nabla^2 p' = \frac{\partial^2}{\partial x_i \partial x_j}[T_{ij}H(f)] - \frac{\partial}{\partial x_i}\{[p_{ij}n_j + \rho u_i(u_n - v_n)]\delta(f)\} + \frac{\partial}{\partial t}\{[\rho_0 v_n + \rho(u_n - v_n)]\delta(f)\} \tag{13}$$

Where, u_i is fluid velocity component in the direction; u_n is fluid velocity component normal to the surface; v_i is surface velocity components in the direction; v_n is surface velocity component normal to the surface; $\delta(f)$ is the Dirac delta function; $H(f)$ is the Heaviside function. p' is the sound pressure at the far field ($p' = p - p_0$). $f = 0$ denotes a mathematical surface introduced to "embed" the exterior flow problem (f > 0) in an unbounded space, which facilitates the use of generalized function theory and the free-space Green function to obtain the solution. The surface (f = 0) corresponds to the source (emission) surface, and can be made coincident with a body (impermeable) surface or a permeable surface off the body surface. n_i is the unit normal vector pointing toward the exterior region (f > 0), a_0 is the far-field sound speed, and T_{ij} is the Lighthill stress tensor, defined as

$$T_{ij} = \rho u_i u_j + p_{ij} - a_0^{\,2}(\rho - \rho_0)\delta_{ij} \tag{14}$$

$$P_{ij} = p\delta_{ij} - \mu\left(\frac{\partial u_i}{\partial x_j} + \frac{\partial u_j}{\partial x_i} - \frac{2}{3}\frac{\partial u_k}{\partial x_k}\delta_{ij}\right) \tag{15}$$

where, p_{ij} is compressible stress tensor, which can be obtained from equation (15) for Stokesian fluid.

$$p'(\overline{x},t) = p'_T(\overline{x},t) + p'_L(\overline{x},t) \tag{16}$$

$$4\pi p'_T(\overline{x},t) = \int_{f=0}\left[\frac{\rho_0\left(\dot{U}_n + U_{\dot{n}}\right)}{\gamma\left(1 - M_r\right)^2}\right]dS + \int_{f=0}\left[\frac{\rho_0 U_n\left\{\gamma \dot{M}_r + a_0(M_r - M^2)\right\}}{\gamma^2(1 - M_r)^3}\right]dS \tag{17}$$

$$4\pi p'_L(\overline{x},t) = \frac{1}{a_0}\int_{f=0}\left[\frac{\dot{L}_r}{\gamma(1 - M_r)^2}\right]dS + \int_{f=0}\left[\frac{L_r - L_M}{\gamma^2(1 - M_r)^2}\right]dS + \frac{1}{a_0}\int_{f=0}\left[\frac{L_r(\gamma \dot{M}_r + a_0(M_r - M^2))}{\gamma^2(1 - M_r)^3}\right]dS \tag{18}$$

$$U_i = v_i + \frac{\rho}{\rho_0}(u_i - v_i) \tag{19}$$

$$L_i = P_{ij}\hat{n}_j + \rho u_i(u_n - v_n) \tag{20}$$

When the integration surface coincides with an impenetrable wall, the two terms on the right in equation(16), $p'_T(\overline{x},t)$ and $p'_L(\overline{x},t)$ are often referred to as thickness and loading terms, respectively, in light of their physical meanings. The square brackets in equation (17) and equation (18) denote that the kernels of the integrals are computed at the corresponding retarded times, τ defined as follows, given the receiver time, t, and the distance to the receiver, r.

$$\tau = t - \frac{r}{a_0} \tag{21}$$

The various subscripted quantities appearing in equation (17) and equation (18) are the inner products of a vector and a unit vector implied by the subscript. For instance, $L_r = \overline{L}.\hat{\overline{r}} = L_i r_i$ and $U_n = \overline{U}.\overline{n} = U_i n_i$, where $\overline{r}$ and $\overline{n}$ denote the unit vectors in the radiation and wall-normal directions, respectively. The Mach number vector M_i in equation (17) and equation (18) relates to the motion of the integration surface: $M_i = v_i / a_0$. The L_i quantity is a scalar product $L_i M_i$. The dot over a variable denotes source.

3.2.2. Möhring Acoustic Analogy:

Solution to sound wave was corresponding to pressure oscillation in inhomogeneous mean flow, and solution to acoustics can satisfy compressible N-S equation.

Acoustic continuity equation is

$$\frac{\partial \tilde{\rho}}{\partial t} + \nabla \cdot (\tilde{\rho}\tilde{v}) = 0 \tag{22}$$

where, ρ is density; v is velocity.

Momentum equation (Crocco's equation) is

$$\tilde{\rho}\frac{\partial \tilde{v}}{\partial t} + \tilde{\rho}\nabla\tilde{B} = \tilde{\rho}\tilde{T}\nabla\tilde{s} + \tilde{\rho}\tilde{v}\times(\nabla\times\tilde{v}) - \nabla\tilde{\tau} \tag{23}$$

where, $\tilde{B}$ is total enthalpy; $\tilde{h}$ is fluid enthalpy; $\tilde{\tau}$ is viscous stress tensor; $\tilde{s}$ is entropy.

Energy equation is

$$\tilde{\rho}\frac{D\tilde{B}}{Dt} - \frac{\partial\tilde{\rho}}{\partial t} = \nabla(\tilde{v}\cdot\tilde{\tau}) + \nabla(\lambda\nabla\tilde{T}) \tag{24}$$

where, $\tilde{T}$ is temperature; λ is thermal conductivity, and the power dissipation caused by heat conduction and viscous stress is neglected. Equation (26) can be deduced from equation (22) and equation (25).

$$\frac{D\tilde{B}}{Dt} = -\frac{1}{\tilde{\rho}}\frac{\partial \tilde{\rho}}{\partial t} \tag{25}$$

$$\frac{\partial \tilde{\rho}}{\partial t} = -\nabla \tilde{\rho}\tilde{v} = \frac{1}{c^2}\frac{\partial p}{\partial t} - \frac{\partial \tilde{\rho}}{\partial \tilde{s}}\frac{\partial \tilde{s}}{\partial t} = \frac{\tilde{\rho}}{c^2}\frac{DB}{Dt} - \frac{\partial \tilde{\rho}}{\partial s}\frac{\partial \tilde{s}}{\partial t} \tag{26}$$

replace $\tilde{\rho}\dfrac{\partial \tilde{v}}{\partial t}$ with $\dfrac{\partial}{\partial t}(\tilde{\rho}\tilde{v}) - \tilde{v}\cdot$ equation (26), we can obtain,

$$\frac{\partial \tilde{\rho}\tilde{v}}{\partial t} - \frac{\tilde{\rho}\tilde{v}}{c^2}\frac{D\tilde{B}}{Dt} + \frac{\partial \tilde{\rho}}{\partial \tilde{s}}\tilde{v}\frac{\partial \tilde{s}}{\partial t} + \tilde{\rho}\nabla \tilde{B} = \tilde{\rho}\tilde{T}\nabla \tilde{s} + \tilde{\rho}\tilde{v}\times(\nabla\times\tilde{v}) - \nabla \tilde{\tau} \tag{27}$$

$$\frac{D\tilde{b}}{Dt} = \rho_T \frac{D\tilde{B}}{Dt} \tag{28}$$

so momentum equation is

$$\frac{1}{\rho_T}\frac{\partial \tilde{\rho}\tilde{v}}{\partial t} - \frac{\tilde{\rho}\tilde{v}}{\rho_T^2 c^2}\frac{D\tilde{b}}{Dt} + \frac{1}{\rho_T}\frac{\partial \tilde{\rho}}{\partial \tilde{s}}\tilde{v}\frac{\partial \tilde{s}}{\partial t} + \frac{\tilde{\rho}}{\rho_T^2}\nabla \tilde{b} = \frac{1}{\rho_T}(\tilde{\rho}\tilde{T}\nabla \tilde{s} + \tilde{\rho}\tilde{v}\times(\nabla\times\tilde{v}) - \nabla \tilde{\tau}) \tag{29}$$

Acoustic propagation equation is

$$\frac{\partial}{\partial t}(\frac{1}{\rho_o c^2}\frac{\partial p}{\partial t}) - \nabla(\frac{1}{\rho_0}\nabla p) = 0 \tag{30}$$

4. Simulation Process

4.1. Computational Domain

The whole sound source domain should be included in computational domain during the simulation process, and which can be obtained from sound source distribution [7]. The ONERA did static testing on several chemical rocket and put forward two variables of L_c and L_a, L_c is laminar core length, m, L_a is effective length in jet flow noise area, m, calculated by equation (31) and (32) respectively.

$$L_c = 1.75 D_j (1+0.38 M_j)^2 \tag{31}$$

$$L_a = 5 L_c \tag{32}$$

We can obtain $L_c = 0.608$ m and $L_a = 5\times0.608 = 3.04$ m by equation (31) and (32) referring to the data in Table 1. In order to seize completely the sound source, the length and diameter of the whole computational domain were set as 4.5 m and 2 m respectively, and the exit central axis of jet nozzle was defined as origin.

4.2. Boundary Conditions

During the simulation, the jet nozzle inlet is defines as pressure inlet, and the side face is defined as far-field pressure, which is a kind of non-reflection boundary condition that can eliminate the sound reflection. Jet nozzle exit is defined as pressure outlet, sound source surface is set as flow field interior surface and inner wall of jet nozzle is set as no-slip boundary conditions.

4.3. Computational Grid

Flow field domain is meshed to five-layer structured "O" grid (see Figure 4). The minimum distance of the grid to jet nozzle interior wall was 5×10^{-6}m, and axial grid is gradually coarsening by 1.5 times. The number of grid nodes is 5,700,000 and there are 15,000,000 hexahedral cells in flow field domain. FW-H sound source surface is 0.15 m distance to outer boundary of flow field (green part in Figure 4 is FW-H sound source surface). Acoustics grid was non-structural tetrahedral (see Figure 5), and there are 2,100,000 acoustics grids. Adaptive grid was used in the calculation and grids automatically refined in pressure jump area. This method was helpful to seize supersonic shock wave structure.
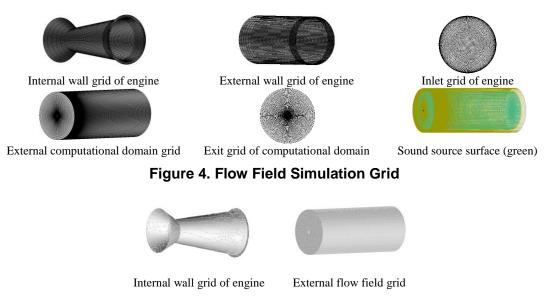
Internal wall grid of engine   External wall grid of engine   Inlet grid of engine

External computational domain grid   Exit grid of computational domain   Sound source surface (green)

Figure 4. Flow Field Simulation Grid

Internal wall grid of engine   External flow field grid

Figure 5. Sound Field Simulation Grid

4.4. Numerical Simulation

The computation is implemented in HP DL580 G7 rack-mounted workstation configuration of the workstation with 64 kernel with 72G memory and 4T hard disk. The ANSYS FLUENT software package is used to solve this problem in double precision solver. During the process of numerical simulation, the time step is set as 2.5×10^{-5} seconds, and each time step iterates 200 times. Since external flow field in large eddy simulation used non-reflection boundary conditions, RNG two equations model is selected firstly to solve the steady compressible N-S equation, and the inlet pressure is increased from 0 MPa to 5.47 MPa in 6 steps. After convergence under the steady state, large eddy simulation is used to solve transient compressible N-S equation with Smagorinsky-Lilly sub-grid model, the second order upwind scheme and density-based double precision coupled solver, about 20 minutes for one step. After computing 200 steps, the flow field parameter become stable. And then set external flow field boundary conditions as pressure far-field boundary conditions and compute 4000 steps until the flow field becomes stable in order to eliminate the effect of the computing under steady state. Finally, compute 2000 more steps, and the fast Fourier transformation and FW-H integration is used to collect sound source and to do frequency analysis; the result of the 2000 steps large eddy simulation is fast Fourier transformed and the noise field is solved and the noise directivity is analyzed by Möhring acoustic analogy. It took about 120 days to complete the whole computation. The simulation process is shown in Figure 6, Computational Aeroacoustics (CAA) collecting data from Computational Fluid Mechanics (CFD) is shown in Figure 7.
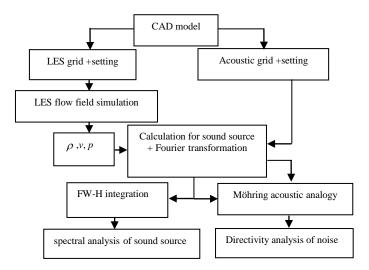
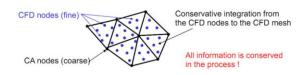**Figure 6. Graphic for Simulation Process**

Figure 7. Data Collection Figure of CFD Result Into CAA

4.4.1. Flow Field Simulation Result

The data of the flow field is collected to analyze the sound field. Accuracy of flow field simulation is very important to guarantee the accuracy of sound field simulation. The result of the flow field simulation are shown in Figure 8 and Figure 9.
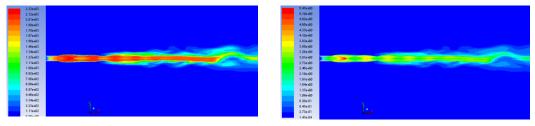

Figure 8. Velocity's Contour

Figure 9. Mach Number's Contour

We can obtain that the velocity is 2005 m/s and Mach number is 2.62 at the exit from Figure 8 and Figure 9, which agree with the data of Table 1. The shock wave was formed inside the flow field, which agrees with major features of supersonic flow too.

4.4.2. Noise Simulation Result

The sound pressure level graph of the noise with frequencies 250Hz and 2500Hz is shown in Figure 10, which is compared with the experimental result shown in Figure 3. The overall sound pressure level of the numerical and experimental results is shown in Figure 11, the biggest difference is 3db, so the simulation method is effective. Figure 12 and Figure 13 are the frequency spectrum curve of 15°and 30° deviating from the central axis.

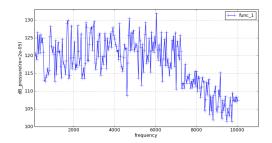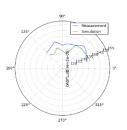**Figure 10. 250Hz And 2500 Hz Sound Pressure Level Graph**

Figure 11. Comparisons Between Test Value And Simulation Value of Overall Sound Pressure Level

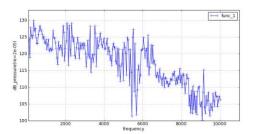**Figure 12. Frequency Spectrum Curve Of 15° Deviating From the Central Axis**

Figure 13. Frequency Spectrum Curve Of 30° Deviating From the Central Axis

The numerical value of low frequency agrees with the experimental results while the high frequency is lower slightly comparing the frequency spectrum curve in Figure 12 and Figure 13 with Figure 2. Since high-frequency noise is formed by small eddy, more refiner grid and the computer resources are needed to collect the high-frequency noise. The sound pressure level of high-frequency noise is lower, which will not cause lager error in computing overall sound pressure level.

5. Conclusions

A method to simulate the missile engine noise is put forward in this paper, which is proved to be effective by comparing the numerical values with the experimental results.

(1) After several attempts, a converging method for computing external flow field by large eddy simulation is set up. The flow field of a small solid fuel engine F is simulated by the large eddy simulation, the numerical results agree with the experimental results tested by NASA and ONERA. An exact results of the flow field calculation is the basis of the following sound field simulation.

(2) The sound field is simulated by conjunction the results of the large eddy simulation with the FW-H surface integration. The numerical results shows that low frequency agrees with the experimental results while the high frequency is lower slightly comparing the frequency spectrum curve.

(3) The flow field results of each time step by large eddy simulation is saved and the time domain data is transformed to the frequency domain data by FFT, then the Möhring acoustic analogy noise direction is analyzed, and the results show that the polar curve of 250Hz and 2500Hz agrees with the test results. A effective method is set up to simulate engine noise directivity by conjunction with the large eddy simulation and Möhring acoustic analogy.

References

[1] K.S. Brentner and F. Farassat, "An Analytical Comparison of the Acoustic Analogy and Kirchhoff Formulations for Moving Surfaces", AIAA Journal, vol. 8, no. 36, **(1998)**.

[2] J. E. Ffowcs Williams and D. L. Hawkings, "Sound generation by turbulence and surfaces in arbitrary motion", Philosophical Transactions of the Royal Society of London, Series A, Mathematical and Physical Sciences, vol. 1151, no. 264, **(1969)**, pp.321-342.

[3] W. Möhring, "A well posed acoustic analogy based on a moving acoustic medium", physics [flu-dyn], vol. 1009, no. 3766, **(2010)**.

[4] J. Varnier, "Experimental study and simulation of rocket engine freejet noise", AIAA Journal, vol. 10, no. 39, **(2001)**, pp.1851-1859.

[5] W. H. Mayes, W E Lanford and H. H. Hubbard, "Near-field and far-field noise surveys of solid-fuel rocket engines for a range of nozzle exit pressures", Va: Largley Research Center Langley Field, **(1989)**.

[6] A. Favre, "Equations des gaz turbulents compressibles », Journal de mecanique, vol. 3, no. 4, **(1965)**.

[7] J. Varnier, W. Raguene and D. Gely, "Noise radiated from free and impinging hot supersonic jets", AIAA-98-2206, **(1998)**.

Authors

Aiqin Li, She received her PhD in School of Aerospace Engineering, Beijing Institute of Technology, China, in 2013. She is currently a lecturer in Beijing Institute of Petro-chemical Technology. Her research interests include jet noise, Industrial furnace thermal properties.

Jiecheng Yu, He received his PhD in School of Aerospace Engineering, Tsinghua University, China, in 2005. He is currently a associate professor at Beijng Institute of Petro-chemical Technology. His research interests include enhanced heat transfer, computational fluid dynamics and numerical heat transfer *etc*.